

This article was downloaded by: [North Carolina State University]

On: 19 January 2013, At: 07:46

Publisher: Taylor & Francis

Informa Ltd Registered in England and Wales Registered Number: 1072954 Registered office: Mortimer House, 37-41 Mortimer Street, London W1T 3JH, UK



## Journal of Hydraulic Research

Publication details, including instructions for authors and subscription information:

<http://www.tandfonline.com/loi/tjhr20>

### Experimental and numerical assessment of the shallow water model for two-dimensional dam-break type problems

Luigi Fraccarollo<sup>a</sup> & Eleuterio F. Toro<sup>b</sup>

<sup>a</sup> Department of Civil and Environmental Engineering, University of Trento, Italy

<sup>b</sup> Department of Mathematics and Physics, Manchester Metropolitan University, U.K.

Version of record first published: 13 Jan 2010.

To cite this article: Luigi Fraccarollo & Eleuterio F. Toro (1995): Experimental and numerical assessment of the shallow water model for two-dimensional dam-break type problems, *Journal of Hydraulic Research*, 33:6, 843-864

To link to this article: <http://dx.doi.org/10.1080/00221689509498555>

PLEASE SCROLL DOWN FOR ARTICLE

Full terms and conditions of use: <http://www.tandfonline.com/page/terms-and-conditions>

This article may be used for research, teaching, and private study purposes. Any substantial or systematic reproduction, redistribution, reselling, loan, sub-licensing, systematic supply, or distribution in any form to anyone is expressly forbidden.

The publisher does not give any warranty express or implied or make any representation that the contents will be complete or accurate or up to date. The accuracy of any instructions, formulae, and drug doses should be independently verified with primary sources. The publisher shall not be liable for any loss, actions, claims, proceedings, demand, or costs or damages whatsoever or howsoever caused arising directly or indirectly in connection with or arising out of the use of this material.

# Experimental and numerical assessment of the shallow water model for two-dimensional dam-break type problems

## Evaluation expérimentale et numérique d'un modèle de Saint-Venant bi-dimensionnel appliquée aux ruptures de barrages



LUIGI FRACCAROLLO

*Research Assistant,  
Department of Civil and  
Environmental Engineering,  
University of Trento,  
Italy*



ELEUTERIO F. TORO

*Professor,  
Department of Mathematics and Physics,  
Manchester Metropolitan University,  
U.K.*

### ABSTRACT

Experimental and numerical results concerning the flow induced by the break of a dam on a dry bed are presented. The numerical technique consists of a shock-capturing method of the Godunov type. A physical laboratory model has been employed to infer properties and validity of the numerical solution. Attention is also given to the applicability of the mathematical model, based on the shallow water equations, to this class of problems.

### RÉSUMÉ

L'article présente les résultats expérimentaux et numériques concernant l'écoulement induit par la rupture d'un barrage sur un lit sec. La technique numérique est celle de la méthode de "shock-capturing" du type Godunov. Un modèle physique en laboratoire a été utilisé pour acquérir des données et valider la solution numérique. Il a été porté une attention particulière à la possibilité d'application du modèle mathématique, basé sur les équations de Saint-Venant, à ce type de problème.

### 1 Introduction

Understanding the basic flow characteristics of dam-break like problems, such as maximum water level, maximum discharge and time arrival curve at assigned locations, though with the help of simplifying assumptions and the use of numerical methods, is fundamental to more reliable engineering design. It is commonly accepted to consider the dam-break problem as a shallow water phenomenon, thus assuming negligible vertical variations of flow properties, except for pressure, which is restricted to be hydrostatic; the model is essentially reduced to a depth-average two-dimensional free surface one. Furthermore, water is assumed incompressible.

There is an acute lack of research effort addressed to investigate and to quantify the validity of the shallow water model. Focussing attention on two-dimensional research, the works of Fennema and Chaudry [6], [7], Valiani [20], Betcheler et al.[4] have to be referred to, because of strong analogies with the physical model considered in the present paper, that is the partial and instantaneous break of a dam. The relevant numerical techniques, based on the conservative form of the model, differ from each other. Fennema and Chaudry [7] compare the explicit methods of MacCormack and

---

Revision received September 22, 1995. Open for discussion till June 30, 1996.

Gabutti. The same authors ([6]) had previously applied an implicit formulation of the Beam-Warming method to the same problem. This is shown to be a robust scheme but their numerical results, in particular the resolution of bores, look highly smoothed. Valiani [20] proposes a semi-implicit extension of the Mac Cormack method, showing how it is possible to modify both the model and the method to evaluate morphological variations on an alluvial erodible bed.

Betcheler et al. [4] applied two different schemes of the artificial viscosity type to the same problem. The first scheme is an explicit predictor-corrector MacCormack method, the second is a method of lines involving central differencing of fluxes in space and Runge-Kutta schemes for the time integration. They also performed experiments to partially validate their numerical results.

Novel numerical techniques have been applied by Yang and Hsu [21]. They used second-order TVD and ENO Riemann-problem based methods. Shock capturing schemes of this type have been exceedingly successful for computing compressible flow. The application they propose consists of the impact of a steep front, moving along a prismatic convergent-divergent channel, on a cylindrical pier. Relevant results confirm the robustness and accuracy of Godunov-type methods.

Alerudo and Garcia-Navarro [1] also used a Riemann-problem based method to solve two-dimensional dam-break type phenomena. They employ a MUSCL type predictor-corrector finite volume scheme on a body-fitted coordinate system, together with a Roe-type approximation to the Riemann problem solution for intercell flux evaluation. No experimental validation of results is presented in this paper.

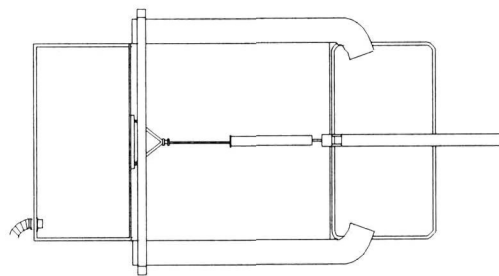
Elliot and Chaudry [5] applied a version of the wave propagation method of Leveque [10]. They tested their numerical results with experimental data for the break of a dam on a straight section, followed by a 180 degree bend and by another straight section (Bell et al. [2]).

As far as experimentation is concerned, accurate measurements have been reported by Bellos et al. [3], who studied dam-break type phenomena in a flume with variable width.

In this paper we report on a numerical and experimental investigation of a three-dimensional dam-break model case. We adopt the two-dimensional shallow water equations as the mathematical description of the problem and apply the Weighted Averaged Flux (WAF) method (Toro [14]). This is a conservative shock-capturing method of the Godunov type that has been successfully applied to the study of shock-wave phenomena. A thorough validation of the numerical results is carried out by utilising experimental data obtained from a purpose built experimental facility. We also used the measured data to assess the applicability of the mathematical model in the form of the two-dimensional depth-averaged shallow water equations.

For this purpose initial data were chosen so as to allow high values of the ratio between vertical and horizontal dimensions. This is crucial to accurately detect important details of the flow and provides a demanding test for the mathematical model being used. The rest of this paper is organized as follows: section two describes the experimental model and the instrumentation; section three describes the numerical method; section four discusses numerical and experimental results. Section five draws conclusions.

Top-view



Side-view

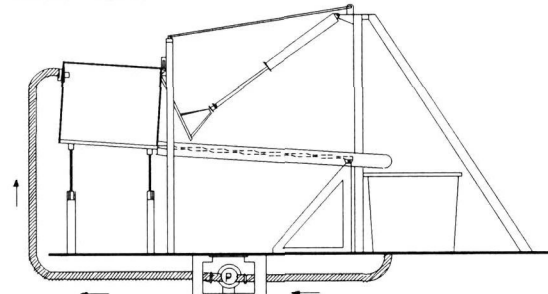
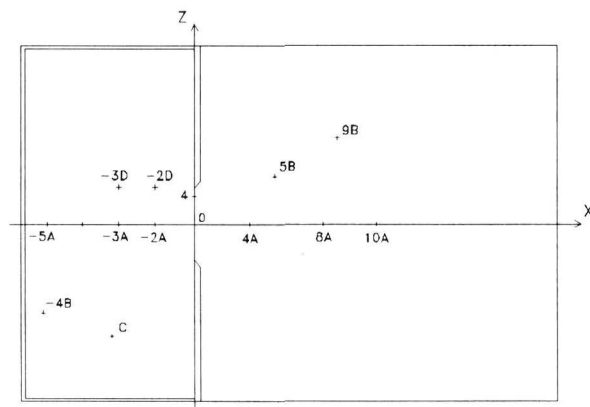


Fig.1. Schematic diagrams of the experimental set-up.



Position	0	4	-5A	-3A	-2A	4A	8A	10A	-4B	5B	9B	C	-3D	-2D
X (cm)	0	0	-82	-42	-22	32.2	72.2	102	-84.5	45.4	80.2	-52	-42	-22
Z (cm)	0	16	0	0	0	0	0	0	-50	25	45	-60	20	20

Fig. 2. Probe positioning with reference to the cartesian plane  $\{x, z\}$ .

## 2 Experimental set-up and instrumentation

In order to simulate a range of three-dimensional dam-break type problems an experimental facility was constructed. The dam rupture is simulated by the sudden removal of a gate and we are interested in the flow phenomena that ensue. The experimental flume is shown in Fig. 1; it consists of a rectangular plane bottom partially occupied, in the longitudinal direction, by a tank on the left hand side. Fig. 1a shows a top view, while Fig. 1b shows a side view. The material used for the walls and the bottom is perspex. This could be useful for flow visualization purposes. Part of the right hand side of the boundary of the tank consists of a rectangular gate placed symmetrically along the center line in the  $x$ -direction. The gate is activated by a pneumatic cylinder, illustrated by Fig. 1b. The downstream part of the plane bottom is initially dry and has open boundaries on all three sides. The whole bottom plate may rotate around a hinge located at its right hand end. This allows to select any desired constant value of the bottom slope. The range of bottom slopes that can be chosen varies between 0% and 10%. The dimensions of the flume are 3.0 m in length and 2.0 m in width. The bottom area occupied by the tank is 1.0 m in the  $x$ -direction and 2.0 m in the transversal direction. The tank can be filled up with water up to a height of 0.80 m, measured along the gate-side wall. The width of the gate, which is symmetrically centered, is 0.40 m. The gate is part of a frame completely separated from the rest of the flume. It rotates around a fixed hinge at its top end, while at the bottom end a pneumatic cylinder applies. This system guarantees a very short opening time of less than 0.1 s, as well as a satisfactory waterproof closure, without the need of gate drivers; these could introduce disturbances into the flow. The thorough separation of the gate frame reduces high frequency vibrations of the flume during the opening process.

The pressures at the bottom of the channel were measured by using pressure gauges, the depths by using wave height meters, and the velocity components by means of an electromagnetic velocity meter. These measurements were carried out at the positions shown in Fig. 2, which includes a table with the relevant  $\{x, z\}$  coordinates.

Wave height meters consist of a pair of stretched nickel/chrome wires, 0.3 mm in diameter, placed parallel to each other at a distance of about 1.0 cm, linked to an electrical circuit; an analogic signal (0–10 Volts) is obtained measuring the electric conductivity of the water depth between the wires. The wire diameter, being very small, causes no significant flow interaction, even in flow regimes close to critical conditions. The response of wave height meters strongly depends on temperature and salt concentration. Calibration is thus required, which must be performed in still water. These difficulties did not allow their use outside the tank, except for position "8A". Furthermore, the gate opening system does not allow the installation of wave height meters in the downstream area of the gate. Pressure gauges measure static pressure values at the bottom. By the hydrostatic assumption they give an indirect evaluation of local depth. The BHL 4310 low range pressure transducer, produced by IMO Transinstruments, has been used. This is connected with a stable bridge amplifier circuit of output signal between 0 ± 10 Volts. Application of pressure gauges by pressure tappings obeys the ISO standard. Preliminary experiments have shown that any mechanical vibration induced on the bottom plate highly affects pressure gauge measurements. This is due to inertial forces applied by the water mass. In order to minimize the effect of unwanted vibrations, the gate-opening system is fully separated from the rest of the experimental apparatus.

As to accuracy of measurements, the maximum relative error for the two kinds of instruments described above does not exceed 1% f.s. values. Repeatability of the measurements, which has been verified also by interchanging the probe positions, is accomplished by the high speed at which the gate is operated.

The  $x$  and  $z$  velocity components were measured by using an E.M.S. gauge. This is a four quadrant electromagnetic velocity meter produced by Delft Hydraulics, that works in the range  $0.0 \div 2.5 \text{ m/s}$  with an accuracy degree of  $\pm 1\%$  f.s. This instrument has good spatial resolution. The sensor is an ellipsoidal disk of 3 cm in diameter that allows simultaneous acquisition of two components of the velocity vector. The instrument is supported by a rounded rod which is to be mounted taking care to avoid possible vibrations induced by the flow.

Data were acquired at a fixed sampling rate of 100 Hz, while typical wave fluctuations during experiments do not exceed a few Hz. Data were converted by a 12 bit analog-digital (A/D) board, 16 channels, and then recorded on a hard disk file.

For the main set of experiments reported in this paper two values of the bottom slope were considered, namely 0 and 7%. All other conditions were kept constant. Initial water depth, measured at the gate, along the normal direction to the bottom, is equal to 60 cm and 64 cm for the horizontal and tilted bottom plane, respectively. In this way the water volume stored in the tank is about the same. Still water was assumed as initial condition in the tank and easily imposed physically. Data acquisition started shortly before the gate opening, so that a few data were available to check initial depth conditions and the correct working of probes. In order to determine the initial time of each experiment, we utilized the pressure gauges and wave height meters at position “0”, which is just upstream of the gate in its initial position. We detected this initial time by looking at the first significant changes of the time-dependent data at position “0”. We found that pressure gauges usually feel the start of the run just a few hundredths of a second before wave height meters do.

The whole recording period for the experiments is equal to 20 s. The influence of different bottom slope values has been evaluated, while dry bed conditions downstream of the dam-gate have been maintained.

### 3 Equations and numerics

Here we present the mathematical model for the class of dam-break problems of our interest and give the details of the technique to compute solutions numerically.

#### 3.1 The shallow water equations

We consider the two-dimensional time-dependent shallow water equations as the mathematical model for the physical situation described in Section 2.

The governing equations, written in differential conservative form, in a cartesian frame of reference, are

$$\mathbf{U}_t + \mathbf{F}(\mathbf{U})_x + \mathbf{G}(\mathbf{U})_z = \mathbf{R}(\mathbf{U}) \quad (1)$$

where  $\mathbf{U}$  is the vector of conserved quantities,  $\mathbf{F}$  and  $\mathbf{G}$  vectors of fluxes given as

$$\mathbf{U} = \begin{bmatrix} \phi \\ \phi u \\ \phi w \end{bmatrix}, \mathbf{F} = \begin{bmatrix} \phi u \\ \phi u^2 + \frac{1}{2}\phi^2 \\ \phi uw \end{bmatrix}, \mathbf{G} = \begin{bmatrix} \phi w \\ \phi uw \\ \phi w^2 + \frac{1}{2}\phi^2 \end{bmatrix} \quad (2)$$

Here  $u$  and  $w$  are the velocity components in the  $x$  and  $z$  directions, respectively,  $\phi$  is usually called the geopotential and is given by

$$\phi = gH$$

where  $g$  is the acceleration due to gravity and  $H$  is the total water depth. The vector  $\mathbf{R}(\mathbf{U})$  contains a number of physical effects such as the bottom slope and friction. Here we take

$$\mathbf{R}(\mathbf{U}) = \begin{bmatrix} R_1 \\ R_2 \\ R_3 \end{bmatrix} = \begin{bmatrix} 0 \\ g\phi(h_x + E_x) \\ g\phi(h_z + E_z) \end{bmatrix} \quad (3)$$

where referred to a fixed datum,  $h$  and  $E$  are the bottom position, increasing downward, and the energy function per unit of weight, respectively. Concerning the energy  $E$  it has been numerically observed that for the model case considered here the bed friction has no influence on the results; we therefore neglect the energy slope term.

The full two-dimensional system of equations (1), with source terms, will be solved numerically in combination with a standard splitting procedure (Toro [19]).

In this way the one-dimensional homogeneous problem

$$\begin{bmatrix} \phi \\ \phi u \end{bmatrix}_t + \begin{bmatrix} \phi u \\ \phi u^2 + \frac{1}{2}\phi^2 \end{bmatrix}_x = \begin{bmatrix} 0 \\ 0 \end{bmatrix} \quad (4)$$

is the basic problem to consider. This can be written as

$$\mathbf{U}_t + \mathbf{F}(\mathbf{U})_x = 0 \quad (5)$$

with the obvious notation for  $\mathbf{U}$  and  $\mathbf{F}(\mathbf{U})$

In order to admit discontinuous solutions the more general integral form of equation

$$\oint (\mathbf{U} dx - \mathbf{F} dt) = 0 \quad (6)$$

is adopted.

### 3.2 Numerical considerations

Given the non-linear character of the shallow water equations and the fact that they admit discontinuous solutions (bores and shear waves), stringent requirements have to be posed on the numerical method to be selected for their solution. In any case the problem is dominated by the propagation of waves carrying strong gradients in the flow. To simulate such phenomena reliably the use of conservative, explicit methods is favoured. To cope with the possible occurrence of bores the use of shock-capturing techniques of the Godunov type, so successful in gas dynamics, is preferred.

Conservative explicit methods for equation (5) are based on the time-marching conservative formula

$$\mathbf{U}_i^{n+1} = \mathbf{U}_i^n + \frac{\Delta t}{\Delta x} \left[ \mathbf{F}_{i-\frac{1}{2}} - \mathbf{F}_{i+\frac{1}{2}} \right] \quad (7)$$

where  $\mathbf{U}_i^n$  denotes the average of  $\mathbf{U}$  in cell  $i$  at time level  $n$ ;  $\Delta t$  is the time-step size and  $\Delta x$  is the width of the cell  $i$  in the  $x$ -direction.  $\mathbf{F}_{i+(1/2)}$  is the numerical flux and represents an approximation to the physical flux function  $\mathbf{F}(\mathbf{U})$  in (5).

Godunov-type methods utilise a local Riemann problem with data  $\mathbf{U}_i, \mathbf{U}_{i+1}$  to compute  $\mathbf{F}_{i+(1/2)}$ .

### 3.3 The Riemann problem

The Riemann problem for (5) is the initial-value problem with initial condition

$$\mathbf{U}(x, 0) = \begin{cases} \mathbf{U}_L, & x < 0 \\ \mathbf{U}_R, & x > 0 \end{cases} \quad (8)$$

The initial data  $\mathbf{U}(x, 0)$  consists of two constant states  $\mathbf{U}_L$  (left) and  $\mathbf{U}_R$  (right) separated by a discontinuity at  $x = 0$ , in local coordinates. This problem does not have a closed-form exact solution, but this can be found iteratively to any desired degree of accuracy (Toro [19]).

The structure of the solution looks as depicted in Fig. 3. There are two waves that separate three constant states. The new state between the left and right waves, called hereafter the “star” state, is determined by the values  $\phi^*$  and  $u^*$ . Both left and right waves can be bores (shocks) or depressions (rarefactions) so that four possible wave patterns result.

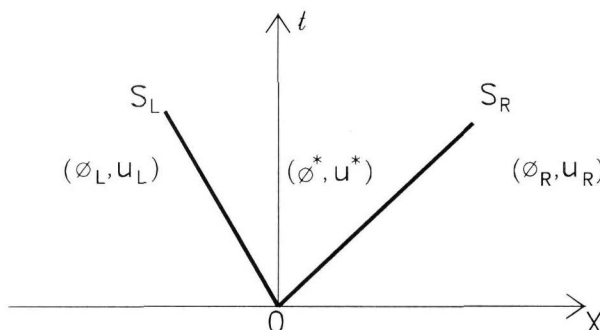


Fig. 3. Structure of the solution of the Riemann problem for the one-dimensional shallow water equations.

The Riemann problem is a generalization of the dam-break problem; the velocities  $u_L$  and  $u_R$  on either side of the initial discontinuity are in general non-zero. The special case in which one of the initial states has no water ( $\phi = 0$ ) results in a wave pattern consisting of one wave only; this is always a rarefaction. The exact solution of this particular case can be found in [16]. An exact and several approximate Riemann solvers to the general case are given in [19]. Here we formulate, implement and assess a Riemann solver of the HLL type.

### 3.4 An HLL-type Riemann solver

Usually, solving the Riemann problem (5),(8) means finding the complete wave structure of Fig. 3, that is, the types of waves present, their strengths and speeds, and the “star” state ( $\phi^*$  and  $u^*$  values). Harten, Lax and van Leer [9] proposed a way of approximately solving the Riemann problem for a general hyperbolic system of the form (5), in a sense to be described. Their approach, called the HLL approach, extracts enough information, in an economical way, to evaluate the intercell flux  $\mathbf{F}_{i+(1/2)}$  directly.

#### 3.4.1 The one-dimensional case

The intercell flux  $\mathbf{F}_{i+(1/2)}$ , here denoted by  $\mathbf{F}_{LR}$ , for most Godunov-type methods depends on the wave speeds  $S_L, S_R$  (Fig. 3). One has

$$\mathbf{F}_{LR} = \begin{cases} \mathbf{F}_L & \text{if } S_L \geq 0 \\ \mathbf{F}^* & \text{if } S_L < 0, S_R > 0 \\ \mathbf{F}_R & \text{if } S_R \leq 0 \end{cases} \quad (9)$$

where  $\mathbf{F}_L = \mathbf{F}(\mathbf{U}_L)$ ;  $\mathbf{F}_R + \mathbf{F}(\mathbf{U}_R)$  and  $\mathbf{F}^*$  is the numerical flux in the star region.

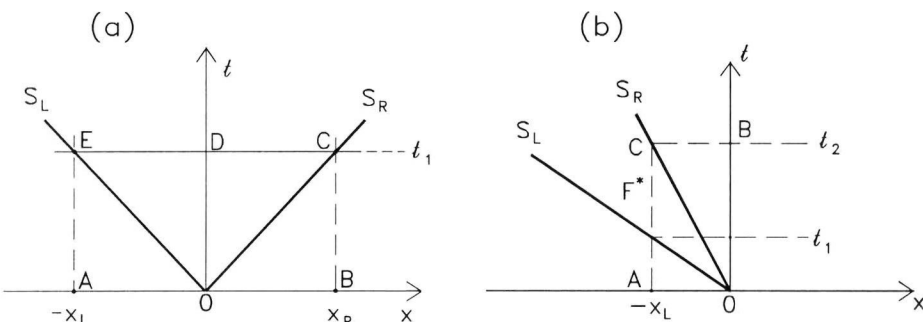


Fig. 4. Wave configuration for the determination of  $\mathbf{F}^*$  using the HLL approach; (a) represents a sub-critical flow and (b) a fully super-critical flow

The Harten-Lax-van Leer approach provides an approximate expression for  $\mathbf{F}^*$  for all flow regimes:  $S_R < 0$ , (left super-critical),  $S_L < 0$  and  $S_R > 0$  (sub-critical) and  $S_L \geq 0$  (right super-critical). The approach requires wave speed estimates  $S_L$  and  $S_R$  for the left and right waves and the integral form 7.

Assume the sub-critical flow configuration of Fig. 4(a), which is characterized by a time  $t_1$  and two positive distances  $x_L$ , and  $x_R$  with  $-x_L = -S_L t_1$ , and  $x_R = S_R t_1$ . Evaluation of integral (6) in the rectangular control volume AODE gives

$$x_L (\mathbf{U}_L - \mathbf{U}^*) = t_1 (\mathbf{F}^* - \mathbf{F}_L)$$

or

$$\mathbf{U}^* = \mathbf{U}_L + \frac{\mathbf{F}^* - \mathbf{F}_L}{S_L} \quad (10)$$

Similarly, evaluation of (6) in control volume OBCD gives

$$\mathbf{U}^* = \mathbf{U}_R + \frac{(\mathbf{F}_R - \mathbf{F}^*)}{S_R} \quad (11)$$

Elimination of  $\mathbf{U}^*$  from (10)–(11) gives

$$\mathbf{F}^* = \frac{S_R \mathbf{F}_L - S_L \mathbf{F}_R + S_L S_R (\mathbf{U}_R - \mathbf{U}_L)}{S_R - S_L} \quad (12)$$

Expression (12) for the flux vector  $\mathbf{F}^*$  is also valid for the cases  $S_R \leq 0$  or  $S_L \geq 0$ , both fully super-critical flows. The details for the case  $S_R \leq 0$  are as follows: consider the wave configuration of Fig. 4(b). There is a positive distance  $x_L$  and two positive times  $t_1$  and  $t_2$ . These are related to the wave speeds  $S_L$  and  $S_R$  by

$$-x_L = -S_L t_1 = -S_R t_2$$

Evaluation of (6) in the rectangular control volume AOBC gives

$$x_L (\mathbf{U}_L - \mathbf{U}_R) = t_1 \mathbf{F}_R - (t_2 - t_1) \mathbf{F}^* - t_1 \mathbf{F}_L$$

Substituting  $t_1 = (S_R/S_L)t_2$ , followed by some algebraic manipulations, gives an expression for  $\mathbf{F}^*$  which is identical to (12). The super-critical case  $S_L \geq 0$  follows in a similar manner.

### 3.4.2 The split two-dimensional case

Computation of two-dimensional flows by Riemann-problem based methods can be carried out by sequences of augmented one-dimensional operators applied successively in the  $x$  and  $z$  directions. For the  $x$  direction the operator is

$$\begin{bmatrix} \phi \\ \phi u \\ \phi w \end{bmatrix} + \begin{bmatrix} \phi u \\ \phi u^2 + \frac{1}{2}\phi^2 \\ \phi uw \end{bmatrix} = \begin{bmatrix} 0 \\ 0 \\ 0 \end{bmatrix} \quad (13)$$

This computational procedure gives rise to a split two-dimensional Riemann problem. It is easy to see that (13) is hyperbolic with real and distinct eigenvalues

$$\lambda_1 = u - \sqrt{\phi}, \lambda_2 = u, \lambda_3 = u + \sqrt{\phi} \quad (14)$$

The solution of the Riemann problem for (13) with data  $\phi_L, u_L, w_L, \phi_R, u_R, w_R$ , has structure as shown in Fig. 5.

An eigenvector analysis shows that the velocity component  $w$  only changes through the middle wave of speed  $S_M = u^*$ . In fact the solution for  $w$  is

$$w(x, t) = \begin{cases} w_L & \text{if } x/t \leq S_M = u^* \\ w_R & \text{if } x/t \geq S_M = u^* \end{cases} \quad (15)$$

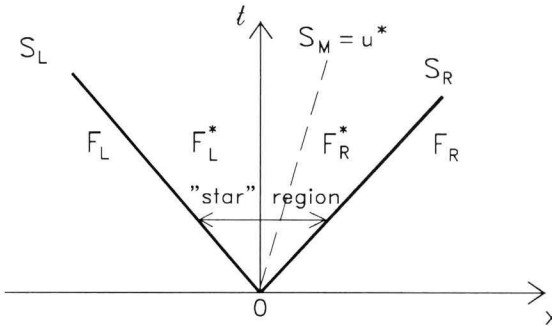


Fig. 5. Wave structure of the split two-dimensional case;  $S_L$  and  $S_R$  are acoustic waves,  $S_m$  is a contact wave.

The solution for  $\phi$  and  $u$  is unaffected by  $w$  and thus the complete solution of the Riemann problem for the split problem (13) is the same as that for (5) with the extra variable  $w$ , the exact solution of which is given by (15). The HLL-type solution is then

$$\mathbf{F}_L^* = \begin{bmatrix} F_1^* \\ F_2^* \\ F_1^* w_L \end{bmatrix}, \mathbf{F}_R^* = \begin{bmatrix} F_1^* \\ F_2^* \\ F_1^* w_R \end{bmatrix} \quad (16)$$

where the meaning of  $\mathbf{F}_L^*$  and  $\mathbf{F}_R^*$  is illustrated in Fig. 5 and flux-vector components  $F_1^*$  and  $F_2^*$  are computed via formula (12). Here we note that (16) is a modified version of HLL flux, as suggested by Toro et al. [15] for Gas Dynamics. The presence of the middle wave is explicit and acknowledged, whereas in the original HLL approach this is neglected.

### 3.4.3 Choice of wave speeds

Key to the success of the HLL approach is the availability of estimates for the wave speeds  $S_L$ ,  $S_M$ , and  $S_R$ . For the shallow water equations there are several possible choices. Some of these were advanced in Toro [19]. Our subsequent experience has shown that use of the two-rarefaction approximation to the solution of the Riemann problem provides simple and reliable estimates. Under this approximation the solution for  $\sqrt{\phi^*}$  and  $u^*$  in the star region (Fig. 5) is direct and is given by

$$\left. \begin{aligned} u^* &= \frac{1}{2} (u_L + u_R) + \sqrt{\phi_L} - \sqrt{\phi_R} \\ \sqrt{\phi^*} &= \frac{1}{2} (\sqrt{\phi_L} + \sqrt{\phi_R}) + \frac{1}{4} (u_L - u_R) \end{aligned} \right\} \quad (17)$$

Estimates for  $S_L$ ,  $S_M$  and  $S_R$ , employing expression (14), are now given by

$$\begin{aligned} S_L &= \min \{ \phi_L - \sqrt{\phi_L}, u^* - \sqrt{\phi^*} \} \\ S_M &= u^* \\ S_R &= \max \{ u_R + \sqrt{\phi_R}, u^* + \sqrt{\phi^*} \} \end{aligned} \quad (18)$$

In addition to its simplicity, choice (18) of wave speed estimates, based on (17), has two more important properties. First it can be shown that  $\phi^* \geq \phi_{exact}$ . This means that choice (18) can be an overestimate of the true wave speeds. This results in enhanced stability. An underestimate of the true wave speeds could be fatal. Another property of (17), (18) concerns vacuum or near vacuum. Certain data in the Riemann problem could lead to negative depth in the star region. This is of course unphysical. The incipient cavitation case, in which  $\phi^* = 0$ , is however physically admissible. Vacuum or near vacuum conditions can be produced by strong rarefactions. But if both non linear waves in the Riemann problem are actually rarefaction waves, then solution (17) is exact, and so is choice (18).

It would be desirable to have an error estimate for  $\phi^*$  and  $u^*$  in (17). However this approach appears to be difficult if all flow regimes are to be considered. On the other hand what is really relevant is the numerical flux that results from the estimated wave speeds (18). Even more relevant is the flux difference in (7), as this is the quantity that directly affects the computed numerical solution. In our experience with shallow water and compressible gas dynamics, even for large errors in  $\phi^*$ , the actual numerical errors in (7) are very small.

#### 3.4.4 The dry-bed case

Here we deal with the special Riemann problem in which one of the data states has no water. There are two cases, namely  $\phi_L > 0$  and  $\phi_R = 0$  (right dry bed) and  $\phi_R > 0$ ,  $\phi_L = 0$  (left dry bed).

In both cases the solution consists of a single rarefaction wave. Two characteristic speeds are significant, namely the left and right bounding wave speeds of the single rarefaction wave. For the right dry bed problem these speeds are

$$\left. \begin{aligned} S_L &= u_L - \sqrt{\phi_L} \\ S_M &= S_R \\ S_R &= u_L + 2\sqrt{\phi_L} \end{aligned} \right\} \quad (19)$$

$S_L$  is the speed of the tail and  $S_R$  the speed of the head of the rarefaction. For completeness we give the solution at a point  $(x, t)$  inside the rarefaction; this is a function of  $x/t$  and is given by

$$\left. \begin{aligned} u &= \frac{1}{3} (u_L + 2\sqrt{\phi_L} + 2x/t) \\ \sqrt{\phi} &= \frac{1}{3} (u_L + 2\sqrt{\phi_L} - x/t) \end{aligned} \right\} \quad (20)$$

For the left dry bed case one has

$$\left. \begin{array}{l} S_L = u_R - 2\sqrt{\phi_R} \\ S_M = S_L \\ S_R = u_R + \sqrt{\phi_R} \end{array} \right\} \quad (21)$$

$$\left. \begin{array}{l} u = \frac{1}{3}(u_R + 2\sqrt{\phi_R} + 2x/t) \\ \sqrt{\phi} = \frac{1}{3}(-u_R + 2\sqrt{\phi_R} + x/t) \end{array} \right\} \quad (22)$$

For numerical entropy satisfaction in the case of a transonic rarefaction, one requires the numerical flux inside the rarefaction wave. This is still denoted by  $\mathbf{F}^*$ , even in the case in which the “star” region coalesces to the tail of the rarefaction ( $\phi = \phi^* = 0$ ).

Again the HLL approach can be applied in a straightforward manner and the result is the same as that given by expression (12). Now the wave speeds given by (19) and (21), the meaning of which is given above, are actually the true speeds of the smallest and largest signals.

The dry bed case puts in evidence the simplicity and power of the HLL type Riemann solver that treats all cases in a unified manner. The peculiarity of each situation is accounted for by the wave speed estimates  $S_L$ ,  $S_M$  and  $S_R$ . The direct use of  $\mathbf{F}^*$  as an approximation to the numerical flux  $\mathbf{F}_{i+(1/2)}$  in (9) gives a version of the first-order accurate method of Godunov. Next, we describe a second-order extension of this method, where  $\mathbf{F}^*$  represents one term in a more accurate numerical flux  $\mathbf{F}_{i+(1/2)}$ .

### 3.5 Review of the WAF method

The Weighted Average Flux (or WAF) method (Toro [14],[19]) has numerical flux

$$\mathbf{F}_{i+\frac{1}{2}}^{\text{WAF}} = \frac{1}{2}(\mathbf{F}_i + \mathbf{F}_{i+1}) - \frac{1}{2} \sum_{k=1}^3 \text{sign}(c_k) A_{i+\frac{1}{2}}^{(k)} \Delta \mathbf{F}_{i+\frac{1}{2}}^{(k)} \quad (23)$$

where

$$\mathbf{F}_i = \mathbf{F}(U_i^n), \Delta \mathbf{F}_{i+\frac{1}{2}}^{(k)} = \mathbf{F}_{i+\frac{1}{2}}^{(k+1)} - \mathbf{F}_{i+\frac{1}{2}}^{(k)}$$

The notation  $\mathbf{F}_{i+(1/2)}^{(k)}$  means the value of the flux function  $\mathbf{F}$  in region  $k$  of the solution of the Riemann problem with data  $\mathbf{U}_i^n, \mathbf{U}_{i+1}^n$ ;  $k = 1$  refers to condition  $\mathbf{U}_L$ , on left side of wave speed  $S_L$  in the  $(x, t)$  diagram,  $k = 2$  to the region between waves  $S_L$  and  $S_M$  and so on up to  $k = 4$ , which refers to state  $\mathbf{U}_R$  (Fig. 5);  $c_k = (\Delta t / \Delta x) S_k$  is the Courant number for wave  $k$ , as  $S_k$  is the speed of wave  $k$ , between state  $k$  and  $k+1$  of the Riemann problem.

$A_{i+(1/2)}^k$  is a numerical viscosity function derived on TVD (total variation diminishing) arguments. Three possible choices are

$$A_S = \begin{cases} 1 - 2(1 - |c_k|), & \text{if } r^{(k)} > 2 \\ 1 - r^{(k)}(1 - |c_k|), & 1 \leq r^{(k)} \leq 2 \\ |c_k|, & \frac{1}{2} \leq r^{(k)} \leq 1 \\ 1 - 2r^{(k)}(1 - |c_k|), & 0 \leq r^{(k)} \leq \frac{1}{2} \\ 1, & \text{if } r^{(k)} \leq 0 \end{cases} \quad (24)$$

$$A_{VL} = \begin{cases} 1, & \text{if } r^{(k)} \leq 2 \\ 1 - \frac{2r^{(k)}}{1 + r^{(k)}}(1 - |c_k|), & \text{if } 0 \leq r^{(k)} \end{cases} \quad (25)$$

$$A_M = \begin{cases} |c_k|, & \text{if } r^{(k)} > 1 \\ 1 - r^{(k)}(1 - c_k), & \text{if } 0 \leq r^{(k)} \leq 1 \\ 1, & r^{(k)} < 0 \end{cases} \quad (26)$$

We call  $A_M$  and  $A_S$  MINA and SUPERA, respectively; they are related to the well known flux limiter functions MINMOD and SUPERBEE (Sweby [13]; Roe [12].  $A_{VL}$  is related to the van Leer flux limiter.

The flow parameter  $r_{i+(1/2)}$  is defined as

$$r^{(k)} = \begin{cases} \frac{\Delta Q_{i-\frac{1}{2}}^{(k)}}{\Delta Q_{i+\frac{1}{2}}^{(k)}}, & \text{if } c_k > 0 \\ \frac{\Delta Q_{i-\frac{3}{2}}^{(k)}}{\Delta Q_{i+\frac{1}{2}}^{(k)}}, & \text{if } c_k < 0 \end{cases} \quad (27)$$

There are two obvious choices for  $Q$ , namely  $Q \equiv \phi$  and  $Q \equiv u$ . Numerical experience suggests that  $Q \equiv u$  is a better choice for two-dimensional shallow water problems.

Details on how the method is extended to solve two-dimensional problems with source terms can be found in Toro [19] and are omitted here.

### 3.6 The CFL stability condition

The choice of the time step size  $\Delta t$  in (7) is subject to the CFL stability constraint

$$\Delta t = C \frac{\Delta x}{S_{max}} \quad (28)$$

where  $0 < C \leq 1$  and  $S_{max}$  is an estimate of the maximum wave speed at the relevant time step. The two-dimensional implementation of the CFL condition requires the replacement of  $\Delta x$  by  $\min\{\Delta x, \Delta y\}$ ; a possible choice for  $S_{max}$  at the time level  $n$  is

$$S_{max} = \max_{i,j} \{ |u_{i,j}^n| + \sqrt{\phi_{i,j}^n}, |w_{i,j}^n| + \sqrt{\phi_{i,j}^n} \}$$

Our experience suggests that this choice is inadequate; it can grossly underestimate the time wave speeds emerging from dam-break like data. This situation is worsened by portions of dry bed. A satisfactory approach is to select  $C$  in (28) small, i.e.  $C \approx 0.1$  during a few time steps after dam rupture and then take  $S_{max} = \max\{S_{max}, S_{RP}^{n-1}\}$  where  $S_{RP}^{n-1}$  is the maximum, in absolute value, of all local Riemann problem speeds  $S_L, S_M, S_R$  at the previous time level  $n - 1$ , in both  $x$  and  $z$  directions. These local speeds are computed for intercell flux evaluation; all the extra work required is to store the maximum value, a single quantity, for the next time step. The constant  $C$  is then set to values close to unity, typically 0.8.

For the class of problems being solved here, in which time accuracy is important and sharp fronts are present in the flow, Godunov-type methods in general are more suitable than other more traditional approaches; they are more accurate and more robust, although they may be less efficient, but this depends crucially on the particular Riemann solver [18]. The one we use is the most efficient available. Amongst Godunov-type method our WAF approach is more accurate than MUSCL type schemes, unless these are enhanced by characteristic limiting [17], which increases their complexity and cost.

## 4 Results

The comparison between measurements and the corresponding numerical results will be presented in this section. A careful inspection on the applicability of the shallow water model to the proposed problem is a necessary step to correctly interpret the numerical results. Attention will be therefore paid also to checking validity and influence of the mathematical hypothesis on the comparison. Numerical results were obtained on a regular mesh of  $150 \times 50$  grid points (along the  $x$  and  $z$  directions, respectively), which preliminary tests have shown to be fine enough.

### 4.1 Free surface and bottom pressure

Data comparison concerning water depth and bottom pressure at the same location enables us to directly check the hydrostatic approximation. Figs. 6 illustrate the experimental free surface displacements, the relevant numerical results and the bottom-pressure measurements at different locations. Only the case  $h_x = 0$  is considered. Graphs are shown until a time duration equal to 10s, the different curves being almost coincident after that. In the tank both the pressure gauges and the

wave height meters were used, while outside it, with one exception, only pressure gauges were applied. Wave height meters yielded a direct free surface evaluation at positions "0", "4", "-5A", "C" and "+8A".

The calculated behaviour of the depth is described, everywhere in the tank, by time dependent curves never monotonically decreasing, but presenting oscillations. This means that the predicted wave activity, though the water volume inside the tank is strictly monotonically decreasing, determines locally a free surface moving alternatively up and down. As far as this numerical characteristic is concerned, there is not agreement between calculations and the measured free surface displacement, which appears much more damped. The only occurrences of rising stages in the measured hydrographs inside the tank concern the positions placed along the gate line ( $z$ -axis). Fig. 6 illustrates the point at the position "0".

Furthermore, the experiments show that there are periods during which the free surface all over the tank is quickly diminishing, alternated with periods in which the free surface seems frozen. This observation is confirmed by velocity measurements to be discussed in the next section.

After the sudden opening of the gate and the start of the flow, strong rarefaction waves moving backward into the tank are originated. As in the one-dimensional case, the water depth at the gate position (e.g., position "0", Fig. 6) reduces drastically to a minimum (about  $\frac{4}{9}$  of the initial depth  $H$ ) after the gate opening. This is analogous to the one-dimensional analytical solution (Ritter [11]) of the frictionless and horizontal dam-break problem (dotted line in Fig. 6). After the minimum the graph shows a rising stage which is due to the contribution of the lateral propagation and represents, therefore, a two-dimensional effect. This aspect is well reproduced numerically. The slight delay of the measured data can be attributed to the fact that actually the gate opening is not instantaneous.

Moving from location "0" towards the backward wall, along the  $x$ -axis, the hydrographs, although showing a similar behaviour, are more and more damped. Fig. 6 also illustrates some stage hydrographs at locations placed outside the  $x$ -axis in the tank, where the reflections of waves on lateral walls does not contribute symmetrically as along the  $x$ -axis.

Under the gate, along the  $z$ -axis, also position "4" was investigated. This is the region where the disagreement between measurements and calculations is larger than elsewhere, because of the shortcomings of the mathematical model. The measured stage hydrographs are above the calculated ones. The pressure-to-depth conversion yields the lowest curve (see graphs at positions "4" and "0", Fig. 6). It can be inferred that, near the gate, the centre of the free-surface curvature radius, on the tangential-normal plane of the intrinsic coordinate system, is beneath the free surface itself. Qualitatively, this situation resembles what happens above a short-crested weir. Besides, the influence of the free surface curvature is strong, so that the three-dimensionality of the flow cannot be neglected.

Moving downward from the gate the free surface curvature, in the intrinsic tangential-normal plane, changes its sign. We note, in fact, that the pressures become greater than the depth-to-pressure converted numerical values. These disagreements between pressures and numerical values can be detected in the positions "4A" and "8A", along the  $x$ -axis, and in the position "5B", outside it (Fig. 6). In this portion of flow domain the pressure values are, during the first two seconds of the test, up to 60% greater than the corresponding numerical ones. Downstream of this region, pressure measurements and calculations produce actually the same results (Fig. 6, pos. "10A" and "9B"). Numerical results are substantiated by the measurements made at the position "8A" (Fig. 6), the only one outside the tank where also a direct measure of depth was performed. Here the effect of the free sur-

face curvature is still present, and numerical and experimental stage hydrographs match satisfactorily.

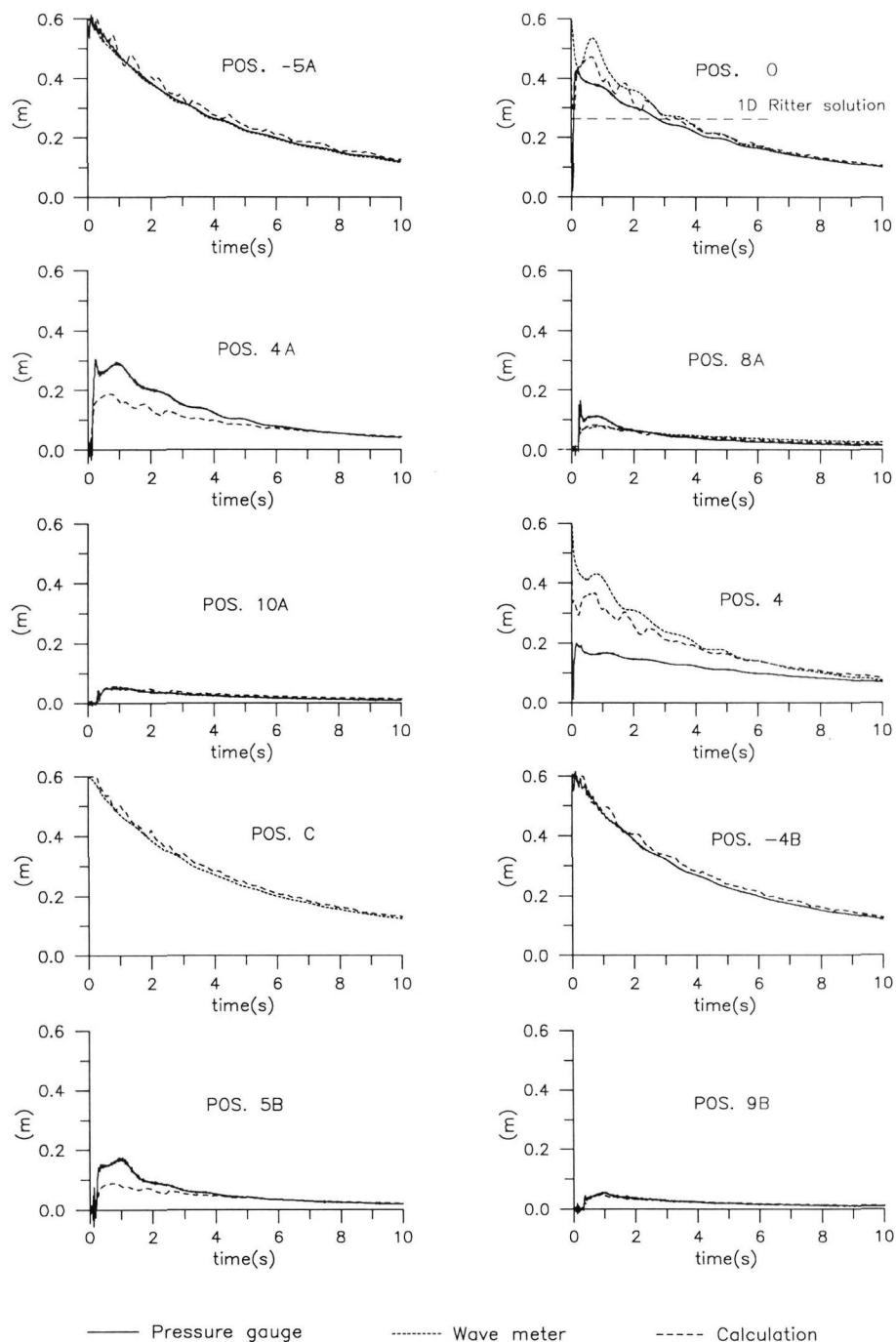


Fig. 6. Calculated and measured stage hydrographs at different positions and the corresponding pressure at bottom, expressed in meters water column; slope = 0.

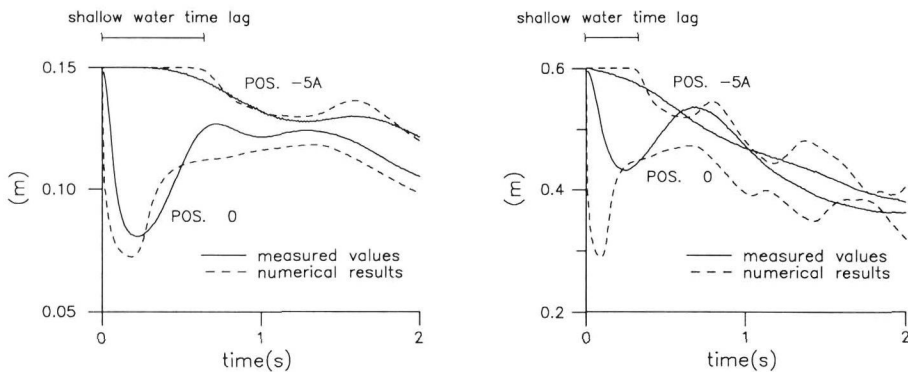


Fig. 7. The expected shallow water time lag of the first detected depth signal between positions “-5A” and “0” is shown in comparison with calculations and measurements. The initial depth is 0.15 m for the left graph and 0.60 m for the right one.

Both the experimental and numerical tests show that the flowing down of water from the tank does not wet the downstream face of the wall adjacent to the gate. The vacuum zone, downstream of the gate edge, is also well reproduced, despite the high value of the free-surface gradients (Fraccarollo and Toro [8]).

Focusing attention on wave speeds, it is surprising that when  $H(t=0) = 0.60$  cm, the signal carrying the first variation on depth, after the gate removal, is observed almost simultaneously everywhere in the tank. By employing different values of the initial depth in the tank the experiments showed that the lower the value of the initial depth in the tank, the better the theoretical prediction. Numerical and experimental results obtained by using different initial depth values are illustrated in Fig. 7. The numerical results predict a time delay among time arrivals of the first signal among different positions in the tank which is consistent with the shallow water equations. The rarefaction waves originated by the dam break move backward at a speed equal to  $\sqrt{gH}$ . The disagreement between theory and data is to be attributed to three-dimensional effects, the importance of which increases as the ratio between vertical and horizontal dimensions of the flow does.

By employing the higher value of the bottom slope, the numerical and experimental results do compare essentially as in the former case. This is expected, since the mathematical and numerical representation of the slope effect is not troublesome. The emptying of the water tank is, of course, faster than before. Fig. 8 displays the effect of the slope by showing together the hydrographs at the positions “-5A” and “0”, both experimentally (left graph) and numerically (right graph). The slope does produce the intersection of the two hydrographs. In fact the values of water depth measured at position “0” become greater than those at “-5A” during last part of the experiment (after about 4 s). This fact is slightly more noticeable numerically.

As far as the propagation of the pressure at the bottom is concerned, the opening of the gate produces an initial quick undershoot on pressure graphs (Fig. 6), which is very strong near the gate (e.g., at position “0”) and reduces progressively moving towards the back wall. The time detection of the first signal change, due to the start of the run, cannot be distinguished from gauge to gauge. This fact induces one to think that a pressure wave is propagating at lower levels (i.e., near the bottom). This observation is also useful to explain the almost simultaneous time detection (already described) of the first depth variation at different locations in the tank.

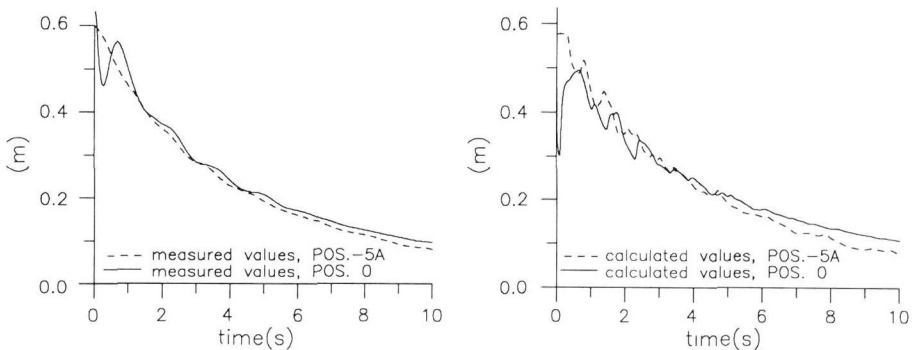


Fig. 8. Calculated and measured stage hydrographs at positions “-5A” and “0”; slope = 7%.

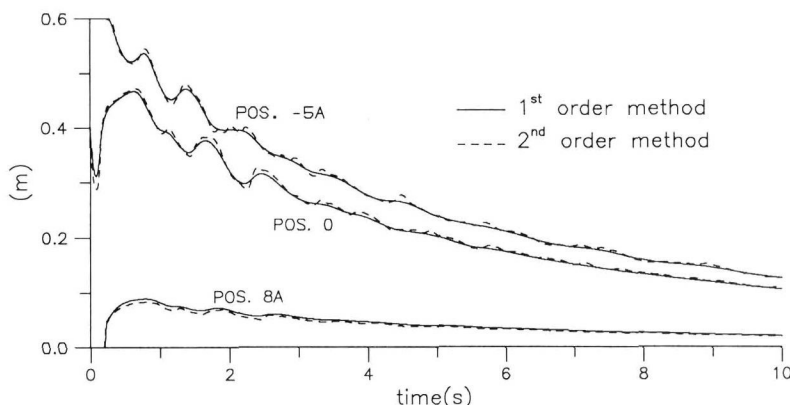


Fig. 9. 1<sup>st</sup> (Godunov) and 2<sup>nd</sup> (present model) order stage hydrographs at different positions.

Non negligible deviations from the shallow water hypothesis induce to think that the proposed model is not the more appropriate tool to reach the goal. Fig. 9 shows a comparison among stage hydrographs at locations “0”, “-5A” and “8A” resulting by applying the present model and a standard first order Godunov method. The conclusion is that the poorer and simpler numerical model can produce results which compare with measured data with about the same rate of accuracy. We can also argue that in real cases, where some further approximations due to the complexity of the problem are to be accepted, a robust first order conservative scheme is good enough to provide the required information.

#### 4.2 Velocity

Difficulties due to the need to avoid vibrations of the rod supporting the velocity sensor prevented the use of the instrument outside the water tank. Furthermore, outside the tank it is necessary to keep free the area facing the gate, in order to allow its rotation during the opening. The only case investigated is where the position of the bottom plane is horizontal (zero slope).

Fig. 10 shows the velocity components diagrams at some of the  $(x,z)$  locations pointed out in Fig. 2. Each graph in the left column of this figure presents a set of eighth curves, each of them referring to a different height from the bottom. They start from level 5cm up to level 40cm, a curve every 5cm. The ending time for each curve is of course different, due to the fact that the free surface, going

down, leaves the gauges outside the flow domain. The right column of the figure presents a comparison between the calculated velocity diagrams (fine line) and the measured velocity average over the depth (bold line); one is to remember that the model assumes a uniform distribution of velocity.

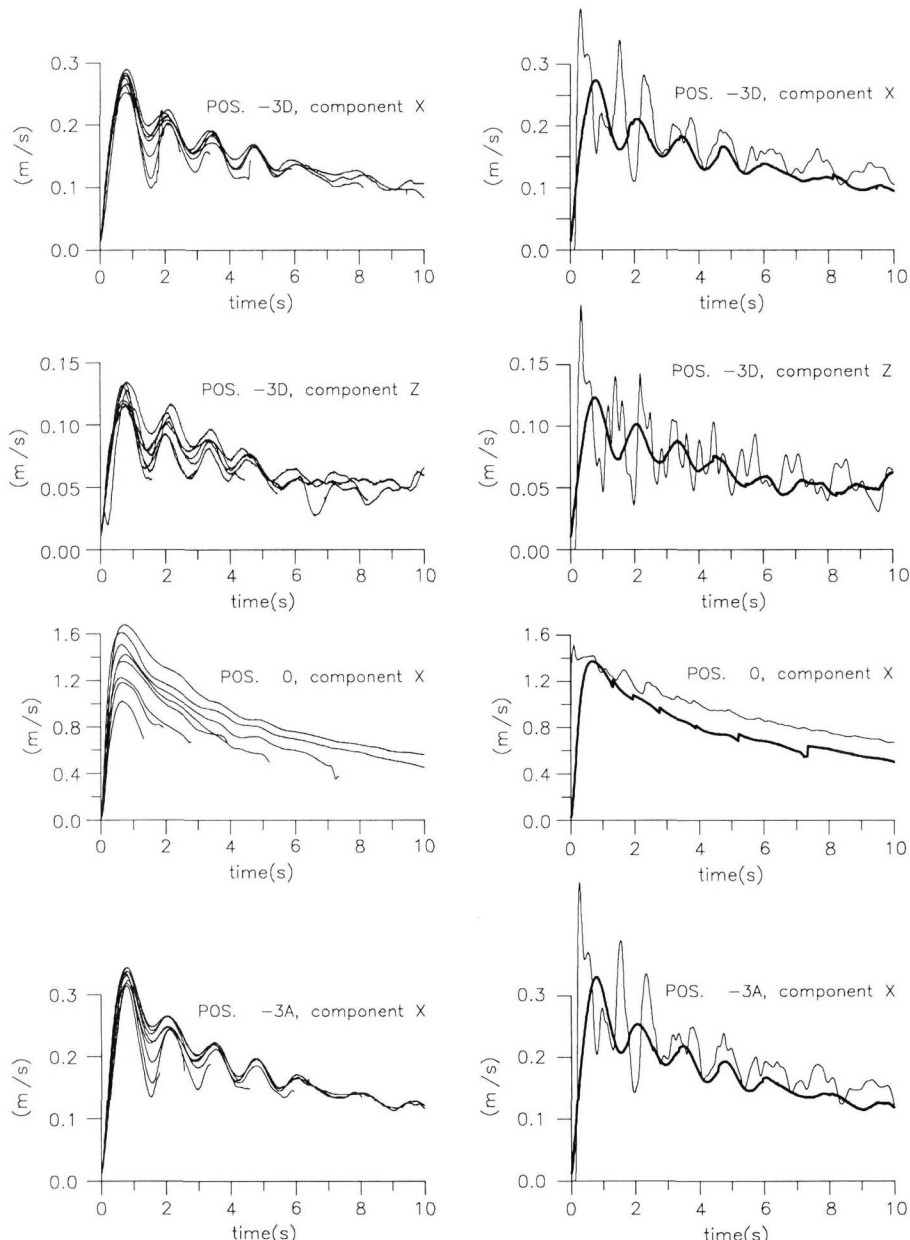


Fig. 10. Measured (left column) and calculated (right column) velocity components at different locations. The bold line curve in the right column represents the measured velocity average over the depth.

It can be inferred that the velocity behaviour is substantially different from the prediction. As far as the measurements are concerned, we observe that in some cases (mainly at locations far from the

gate), the graphs exhibit strong oscillating features. The relevant frequency value, inferred by considering subsequent peaks, is equal to about  $1.25\text{Hz}$ , the same at all positions. At location “0”, the velocity, after having reached the maximum value, decreases more or less monotonically. Curves relevant to different levels, at the same location behave similarly. Furthermore, not only at the same location, but also at different locations, the velocity signals oscillate with small phase-angle differences (e.g., see the sequence of positive peaks at different positions). It is easy to recognize the correspondence between high velocity and free surface fast diminishing phases; viceversa, low velocity phases correspond to bumps in the stage hydrographs. Interesting enough, in the tank the character of the flow is throughout sub-critical.

The model predicts a velocity field which is often in the range described by the measurements taken at different levels for each location. According to the physical situation, also the calculations show an oscillating behaviour of the velocity components which is, nevertheless, more irregular than the real one. The amplitude of the oscillations is somewhere, at the beginning, even twice the measured one (e.g., see the  $z$ -component at the position “-3D” or the  $x$ -component at the position “-3A” of Fig. 10).

The knowledge of velocity at different levels allows us to approximate the value of the Coriolis coefficients  $\beta_1$ ,  $\beta_2$  and  $\beta_3$ . These are the non-dimensional coefficients in the convective terms of the momentum equations. These are:  $\beta_1 = \frac{1}{H\bar{u}^2} \int_0^H uudz$ ;  $\beta_2 = \frac{1}{H\bar{u}\bar{w}} \int_0^H uw dz$ ;  $\beta_3 = \frac{1}{H\bar{w}^2} \int_0^H wwdz$ , where the overbar indicates the depth-averaged value. These coefficients are assumed equal to one in the mathematical model, according to the uniformity assumption. The time depending graphs of the measured  $\beta_1$  and  $\beta_3$ , at some positions in the tank, are represented in Fig. 11.

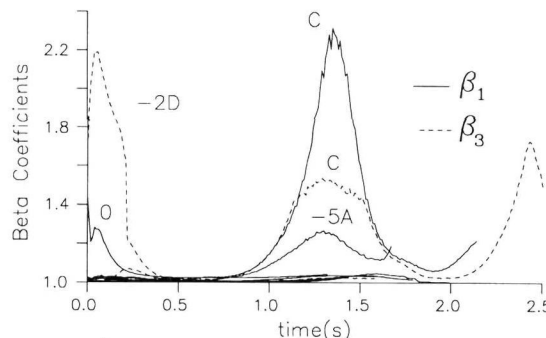


Fig. 11. Coriolis  $\beta$ -coefficients at different positions. Curves close to unity are specified in the text.

Some of the curves, actually not distinguishable in the figure, are close to the value 1. They are the  $\beta_1$  curves at the positions “-3D”, “-3A”, “-2D”, “-2A”, and the  $\beta_3$  one at the position “-3D”(not considering for  $\beta_3$  the positions on the  $x$ -axis, where  $u$  is null).

## 5 Conclusions

The aim of the present work was the proposition and validation of a 2nd order accurate numerical scheme of the Godunov type for the two-dimensional shallow water equations. It was tested under very severe conditions, allowing the flow to be sonic or critical, and choosing a dry bed as initial condition downstream of the gate. The scheme is successfully both in terms of stability and accuracy. An experimental model of a dam-break was constructed to assess the validity of the mathematical and numerical representations.

The paper highlights the features of the flow case. Summarizing, the high free surface gradient near the gate produces substantial deviations from the shallow water assumptions. It was checked how and where pressure and velocity distributions deviate from the shallow water hypothesis. The calculated free surface displacements presents some characteristics which are not consistent with observations.

In spite of that, the present scheme was proved able to simulate satisfactorily the main features of the flow.

## References / Bibliography

1. ALCRUDO F. and GARCIA-NAVARRO P., *A high resolution Godunov-type scheme in finite volumes for the 2D shallow water equations*, Int. Journal for Numerical Methods in Fluids, Vol. 16, 489–505, 1993.
2. BELL S. W., ELLIOT R. C. and CHAUDRY M. H., *Experimental results of two-dimensional dam-break flows*, Journal of Hydraulic Research, Vol. 30, N.2, 225–252, 1992.
3. BELLOS C. V., SOULIS J. V. and SAKKAS J. G., *Experimental investigation of two-dimensional dam-break induced flows*, Journal of Hydraulic Research, Vol. 30, N.1, 47–63, 1992.
4. BECHTELER W., KULISH H. and NUJIC M., *2-D dam-break flooding waves comparison between experimental and calculated results*, 3rd International Conference on “Floods and Flood Management”, Florence 24–26 November, 247–260, 1992.
5. ELLIOT R. C. and CHAUDRY M. H., *A wave propagation model for two-dimensional dam-break flows*, Journal of Hydraulic Research, Vol. 30, N.4, 467–483, 1992.
6. FENNEMA R. J. and CHAUDRY M. H., *Implicit method for two-dimensional unsteady free-surface flows*, Journal of Hydraulic Research, Vol. 27, N. 3, 321–332, 1989.
7. FENNEMA R. J. and CHAUDRY M. H., *Explicit method for 2-D transient free-surface flows*, Journal of Hydraulic Engineering, Vol. 116, N. 3, 1013–1034, August 1990.
8. FRACCAROLLO L. and TORO E. F., *A shock-capturing computational method for two dimensional dam-break type problems*, Proceedings of the 5th International Symposium on Computational Fluid Dynamics, Tohoku University, Sendai, Japan, Vol.I, 178–183, August 31–September 3, 1993.
9. HARTEN A., LAX P. D. and VAN LEER B., *On upstream differencing and Godunov-type schemes for hyperbolic conservation laws*, SIAM Review, N. 25, 35–61, 1983.
10. LEVEQUE R. J., *A large time step generalization of Godunov's method for system of conservation laws*, SIAM J. Num. Anal., 22, N.6, 1051–1073, 1985.
11. RITTER A., *Die Fortplanzung der Wasserwellen*, Zeitschrift des Vereines Deutscher Ingeniere, 36(33), 947–954, 1992.
12. ROE P., *Some contributions to the modelling of discontinuous flows*, Lectures in Applied Mathematics, 22, 163–193, 1985.
13. SWEBY P. K., *High resolution schemes using flux limiters for hyperbolic conservation laws*, SIAM J. Num. Anal., 21, 995–1011, 1984.
14. TORO E. F., *A weighted averaged flux method for hyperbolic conservation laws*, Proc. R. Soc. Lond. A423, 401–418, 1989.
15. TORO E. F., SPRUCE M. and SPEARES W., *Restoration of the contact surface in the HLL-Riemann solver*, Shock Waves, Vol. 4, 25–34, 1994.
16. TORO E. F., *The dry-bed problem in shallow-water flows*, CoA Report N.9007, Cranfield Institute of Technology, Cranfield, U.K., 1990.
17. TORO E. F., *MUSCL-type primitive variable schemes*, Tech. Rep. MMU-9501, The Manchester Metropolitan Univ., Dpt. of Mathematics and Physics, Manchester, U.K., 1995.
18. TORO E. F., *Riemann solvers and upwind methods for fluid dynamics*, Springer-Verlag (to appear in 1996).
19. TORO E. F., *Riemann problems and WAF method for solving the two-dimensional shallow water equations*, Phil. Trans. R. Soc. Lond., 338, 43–68, 1992.
20. VALIANI A., *Un modello numerico semiimplicito per la trattazione di bruschi transitori in moti a superficie libera e fondo mobile*, 23\_ Convegno di Idraulica e Costruzioni Idrauliche, Florence 31 August–4 September, Vol. E, 261–276, 1992.
21. YANG J. Y. and HSU C. A., *Computations of free surface flows*, Journal of Hydraulic Research, Vol. 31, N. 3, 321–332, 1993.

## Notations

$\mathbf{F}, \mathbf{G}$	vectors of fluxes
$\mathbf{R}$	vector of source terms
$\mathbf{U}$	vector of conserved variables
$u, w$	velocity components
$\phi$	geopotential
$h$	bottom elevation
$\phi^*, u^*$	the star state of the Riemann problem solution
$S_L, S_R, S_M$	wave speeds of the Riemann problem
$x, z$	spatial coordinates
$t$	time
$c_k$	Courant number
$\beta_i$	Coriolis coefficient